Boundary condition of grounding lines prior to collapse, Larsen-B Ice Shelf, Antarctica

M. Rebesco *et al.*

Science **345**, 1354 (2014);
DOI: 10.1126/science.1256697

ICE SHEETS

Boundary condition of grounding lines prior to collapse, Larsen-B Ice Shelf, Antarctica

M. Rebesco,[1] E. Domack,[2,3]* F. Zgur,[1] C. Lavoie,[1,4] A. Leventer,[5] S. Brachfeld,[6] V. Willmott,[7] G. Halverson,[8] M. Truffer,[9] T. Scambos,[10] J. Smith,[11] E. Pettit[12]

Grounding zones, where ice sheets transition between resting on bedrock to full floatation, help regulate ice flow. Exposure of the sea floor by the 2002 Larsen-B Ice Shelf collapse allowed detailed morphologic mapping and sampling of the embayment sea floor. Marine geophysical data collected in 2006 reveal a large, arcuate, complex grounding zone sediment system at the front of Crane Fjord. Radiocarbon-constrained chronologies from marine sediment cores indicate loss of ice contact with the bed at this site about 12,000 years ago. Previous studies and morphologic mapping of the fjord suggest that the Crane Glacier grounding zone was well within the fjord before 2002 and did not retreat further until after the ice shelf collapse. This implies that the 2002 Larsen-B Ice Shelf collapse likely was a response to surface warming rather than to grounding zone instability, strengthening the idea that surface processes controlled the disintegration of the Larsen Ice Shelf.

Our ability to model or predict changes in marine-based glaciers or ice sheets due to warming temperatures or rising sea level is limited by an inadequate understanding of the character of ice shelf/ice sheet grounding zone systems (GZSs) (*1*–*3*). Atmosphere and seawater temperature variation force changes in ice mass transfer to the oceans (*4*); however, the removal of ice shelf buttressing is also critical in regulating glacier response (*5*–*7*). In February to March of 2002, the Larsen-B Ice shelf (LIS-B) catastrophically collapsed, with a loss of ~3250 km^2 of floating ice (*8*). Tributary glaciers that had fed into the ice shelf system—including the Crane and Hektoria Glaciers—accelerated considerably after the collapse (*5*–*7*). After this was a rapid recession of the ice-calving fronts of the glaciers and transition to a tidewater glacier character (*9*). The events revived the thinking that linkages between grounded glaciers and ice shelves are indeed critical, more so than recently assumed (*10*), but underscored the need for detailed knowledge of the characteristics of GZSs and GZS transitions in ice-shelf and tidewater glacier systems.

A swath bathymetry survey in 2006 imaged the inner-shelf sea floor of the Larsen-B embayment that was exposed after the ice shelf collapse (Fig. 1A). The extensive arcuate GZS at the entrance to Crane Fjord is a large sedimentary prism seaward of a local bathymetric divide, which has a variable depth between 690 and 660 m. The grounding zone to the south appears to run parallel to a terrace at 600 m depth, whereas its expression in the drainage of the Jorum/Punchbowl system is less clear because of the steep crystalline bedrock slope that dominates the intervening headland (*11*). The GZS prism tapers relatively gently seaward and is steeper landward. Elongated ridges subparallel to the axis of the Crane Fjord, similar to subglacial lineations observed elsewhere on the Antarctic margin (*12*, *13*), are interpreted as fluted subglacial bedforms [such as mega-scale glacial lineations (MSGLs)]. A series of furrows curve toward the southeast as a result of the ice flow from the Jorum/Punchbowl system, and a pad of fluted sediment marks the central axis of the Crane Fjord. A set of relict channels (in an irregular pattern of salients and reentrants) also appears to crosscut the arcuate furrows on both the lee and stoss side of the GZS. These features collectively mark episodes of decoupling from the GZS, beginning with the formation of the arcuate ridges, followed by cross-cutting of channels and then deposition of the central fluted pad of sediment.

Sediment cores from the Larsen B embayment address the question of whether this GZS served to anchor the LIS-B before its 2002 collapse. Core NBP0603 KC-10 was recovered from the top of the GZS. The boundary between the diamicton (Unit 1) and the overlying sediments dates back at least 11,000 years (Fig. 2 and supplementary materials), indicating that this GZS was abandoned at termination I. The timing of glacial ice liftoff is supported further by a radiocarbon-based chronology from three other sediment cores, where the same stratigraphy was observed (Figs. 2 and 3). These observations of the GZS do not agree with the location of the grounding zone as inferred from satellite images (*14*), and the sediment core data reveal that glacial ice was not grounded here immediately before the 2002 LIS-B collapse. The reason for the misplacement of the grounding line by (*14*) is unclear, but thick floating ice inside a relatively narrow channel would exhibit reduced tidal bending, as would have been the case with the Crane Glacier at this time. It is possible that a rift and/or structural arch in this area would mimic the appearance of a grounding line. The abandonment of the large GZS relatively early (before 11.7 thousand years ago) with respect to Holocene events suggests that retreat of grounded ice within the LIS-B embayment was driven by processes similar to those that drove shelf-wide recession across the NW Weddell Sea continental shelf (*15*). We suggest that this innermost retreat into the deep troughs of the Nordenskӧld Coast was tied to late stages of global eustatic forcing coupled to retreat of global glacial cover. The sedimentology and facies relationships of sediment cores just seaward of the Crane Trough (in Exasperation Inlet) demonstrate a rapid recession of the ice sheet system across the inner shelf, which occurred 12.5 thousand years ago (Figs. 2 and 3 and fig. S1). The chronologic data we present (table S1), combined with existing published data further seaward (*11*), establish recessional rates of the grounding line within the main axis of the LIS-B embayement of ~100 m/year during the period from 12.3 thousand to 11.7 thousand years ago, comparing favorably with ice sheet/shelf recessional rates obtained for the same period in the western Ross Sea (*16*).

Further, geophysical data, combined with Advanced Spaceborne Thermal Emission and Reflection Radiometer (ASTER) imagery, can be used to determine the location of the LIS-B pre-collapse grounding line in the Crane Fjord (Fig. 1). The Crane Trough consists of three very deep (>1000 m) and narrow (~1 km wide) elongated basins separated by more elevated crests, each representing the threshold of the upslope basin. The floor of the basins shows a flat morphology, which is typical of a subsequent sedimentary filling under subaqueous conditions. The upper basin is not fully charted and shows the presence of MSGLs subparallel to the axis of the fjord. We interpret this morphology as the result of deposition of till beneath grounded ice. On Arctic continental margins, the same interpretation is given to similar associations of thresholds and MSGLs (*17*). The fact that the ice was grounded in the fjord is confirmed by the single-channel seismic data, whose landward overdeepening and stairway

[1]Istituto Nazionale di Oceanografia e di Geofisica Sperimentale (OGS), Borgo Grotta Gigante 42/C-34010, Sgonico (TS) Italy. [2]Department of Geosciences, Hamilton College, Clinton, NY 13323, USA. [3]College of Marine Science, University of South Florida, 140 7th Avenue South, St. Petersburg, FL 33701-5016, USA. [4]Centre for Environmental and Marine Studies/Department of Geosciences, University of Aveiro, Aveiro 3810-193, Portugal. [5]Department of Geology, Colgate University, Hamilton, NY 13346, USA. [6]Department of Earth and Environmental Studies, Montclair State University, Montclair, NJ 07043, USA. [7]International Cooperation, Alfred-Wegener-Institut Helmholtz-Zentrum für Polar-und Meeresforschung. Am Handelshafen 12, 27570 Bremerhaven, Germany. [8]Earth and Planetary Sciences, McGill University, Montreal, Quebec H3A 2A7, Canada. [9]Geophysical Institute, University of Alaska Fairbanks, Fairbanks, AK 99775, USA. [10]National Snow and Ice Data Center, University of Colorado, Boulder, CO 80309, USA. [11]British Antarctic Survey, Cambridge CB3 0ET, UK. [12]Department of Geosciences, 900 Yukon Drive, Room 308, Post Office Box 755780, University of Alaska Fairbanks, Fairbanks, AK 99775, USA.
*Corresponding author. E-mail: edomack@usf.edu

geometry between its three basins can be explained best by the carving action of ice (*18*). The 2001 ASTER Digital Elevation Model (DEM) profile locates the pre-collapse grounding zone of the Crane Glacier portion of the LIS-B at the threshold between the upper and the middle basin, >13 km from the large GZS described above (Fig. 1B). The stability of the LIS-B through the Holocene (*10*) thus was not dependent on grounding at a large GZS; instead, collapse was forced by surface melt processes (*6*).

Well-layered, undisturbed sediments extend for at least 40 m below the lower (outermost) basin (Fig. 4). This thickness is exceptional for an inner-shelf deposystem that has been covered by an ice shelf until only a few years ago (*19*). Seismic data show that the layered fill is underlain by at least two other seismic units of variable thickness and complexity (Fig. 4). In dip profile, this wedge-shaped unit slopes rapidly landward, beneath the middle basin, and subsequently dips seaward beneath the layered fill of the lower basin. Internally, it shows mounded, low-amplitude reflectors terminating landward with marked downlap and seaward progradation. In strike, the sediments at the base of this unit have a relatively high sound velocity (~1700 m/s), as indicated by the analysis of the diffraction hyperbolas. The lowest identified unit is more complex, poorly defined, and characterized by hummocky, irregular, high-amplitude reflectors. Its top shows alternating ridges and troughs in strike profile, which match the morphology of the thresholds between each basin.

The above observations allow us to reconstruct the relative succession of events that generated the sedimentary deposits within the Crane Fjord. Similar to other overdeepened basins on the Antarctic inner shelf (*20*), this fjord has been carved, likely along structural lines of weakness, by grounded ice. The last time the ice was grounded within the fjord is represented by the top of the lowest identified unit (Fig. 4). Its geometry of alternating troughs and ridges matches subglacial bedforms exposed across adjacent

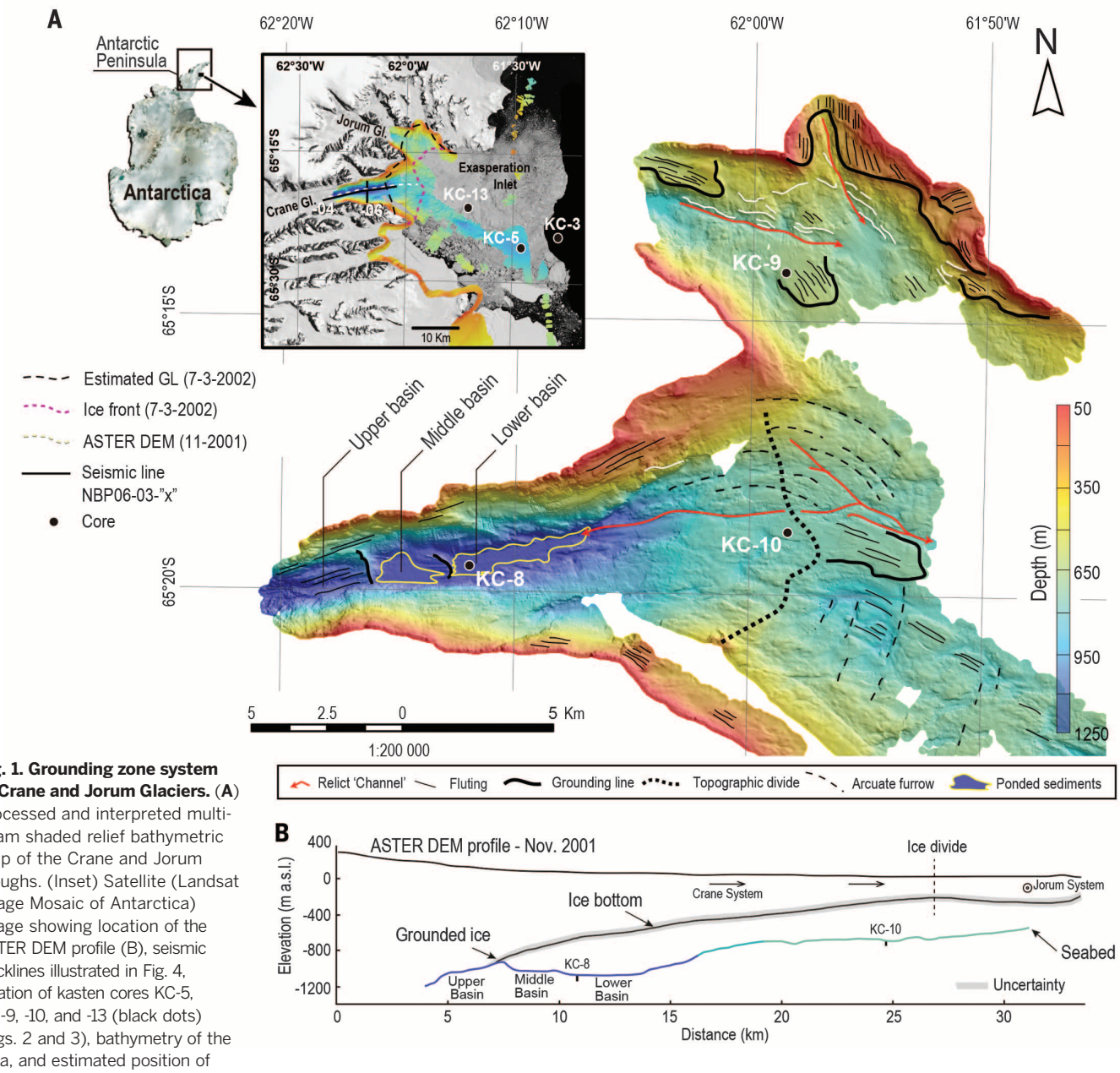

Fig. 1. Grounding zone system of Crane and Jorum Glaciers. (**A**) Processed and interpreted multibeam shaded relief bathymetric map of the Crane and Jorum Troughs. (Inset) Satellite (Landsat Image Mosaic of Antarctica) image showing location of the ASTER DEM profile (B), seismic tracklines illustrated in Fig. 4, location of kasten cores KC-5, -8, -9, -10, and -13 (black dots) (Figs. 2 and 3), bathymetry of the area, and estimated position of grounding line (dashed black line) after (*14*). (**B**) ASTER DEM profile of the LIS-B just before its breakup, and the underlying bathymetry derived from the multibeam data. Before collapse of the ice shelf in 2002, the ice is grounded just landward of the middle ponded basin.

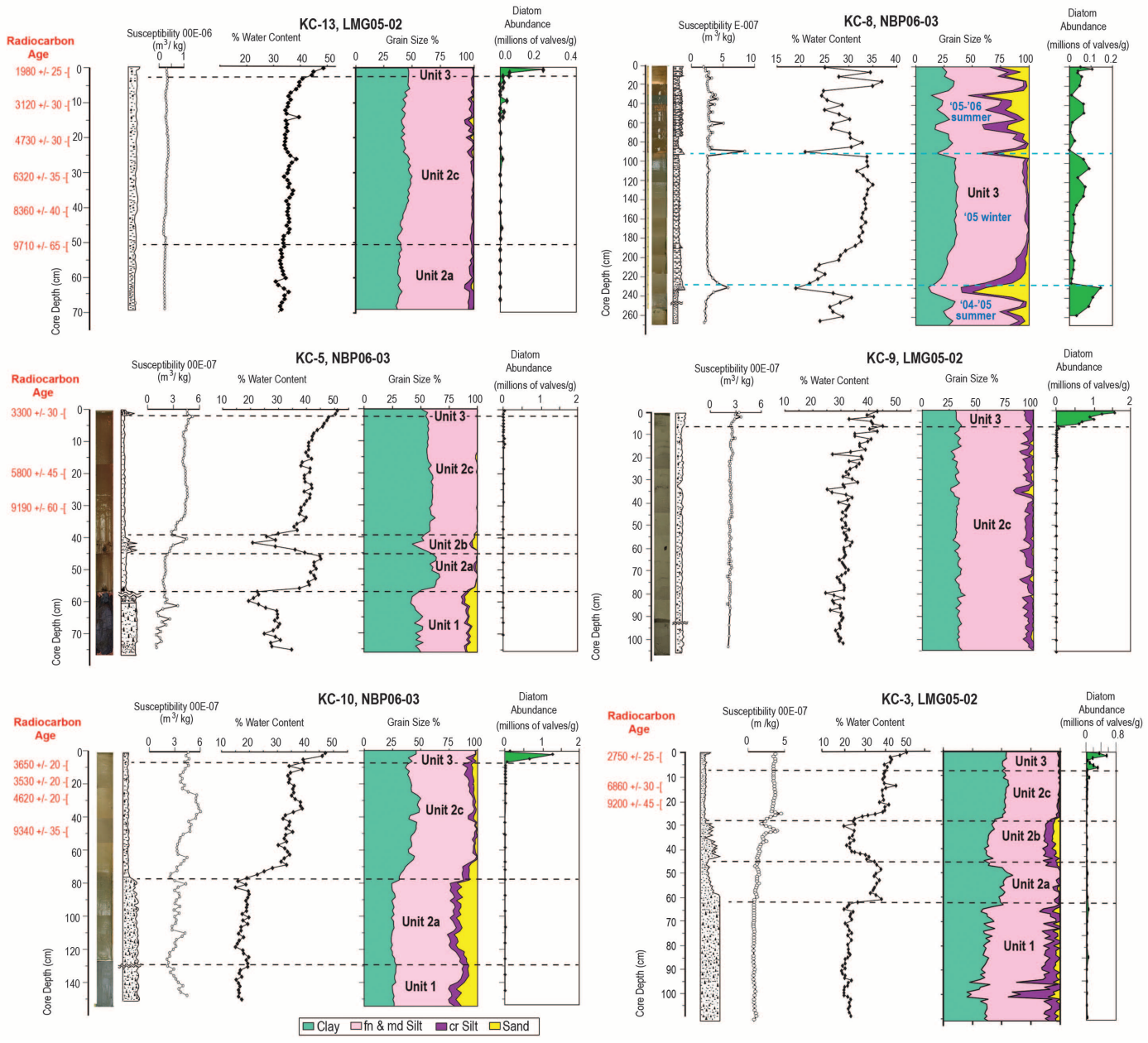

Fig. 2. Photographs, lithofacies, physical properties, and diatom abundance for six kasten cores collected in the vicinity of the Crane Trough. The locations of the cores are depicted in Fig. 1. Unit designations are as follows: Unit 1 is glacial diamicton (till) related to ice sheet (ice stream) grounding upon sea floor; Unit 2 is sub–ice shelf sediment related to near (proximal) grounding line (2a), distal to grounding line (2c) and an, as yet, undetermined coarse interval (2b); and Unit 3 represents the seasonal open marine facies formed since the break up of the LIS-B. Uncorrected radiocarbon dates on foraminiferal calcite (table S1) are indicated in red.

thresholds. Furthermore, the hummocky character of underlying reflectors is consistent with deposition of subglacial till at the glacial bed. Conversely, the overlying wedge-shaped unit with its top sloping rapidly landward suggests the development of a grounding zone, beyond which a body of water separated the base of the ice from the sea floor, such as a "subglacial lake" (*21*). Its geometry and the internal prograding reflectors resemble those of subglacial deltas identified elsewhere along Antarctic grounding zones (*20*). This delta may have developed in a subglacial lake setting similar to that inferred for features in the Northern Prince Gustav Channel (*13*) and the Palmer Deep basin (*19*, *22*).

The overlying layered seismic unit was clearly deposited subaqueously. Core KC-8 collected near the intersection of profiles NBP0603-04 and -06 (Figs. 1 and 3) suggests that the uppermost sediments resulted from the accelerated ice discharge (rafting) from the Crane Glacier after the breakup of LIS-B and seasonal slumping of debris along the flanks of the Crane Fjord (fig. S2). This 2.7-m core shows clear meter-scale grain-size alternation between a fine silt facies (virtually devoid of sand) and a sandy silt facies (sand fraction up to >50%) (Fig. 2). The presence of well-preserved diatoms commonly associated with the sea ice environment suggests that the entire 2.7-m-thick sequence was deposited in open marine conditions with annual sea ice (not sub–ice shelf)—conditions that are known to have been present only since austral

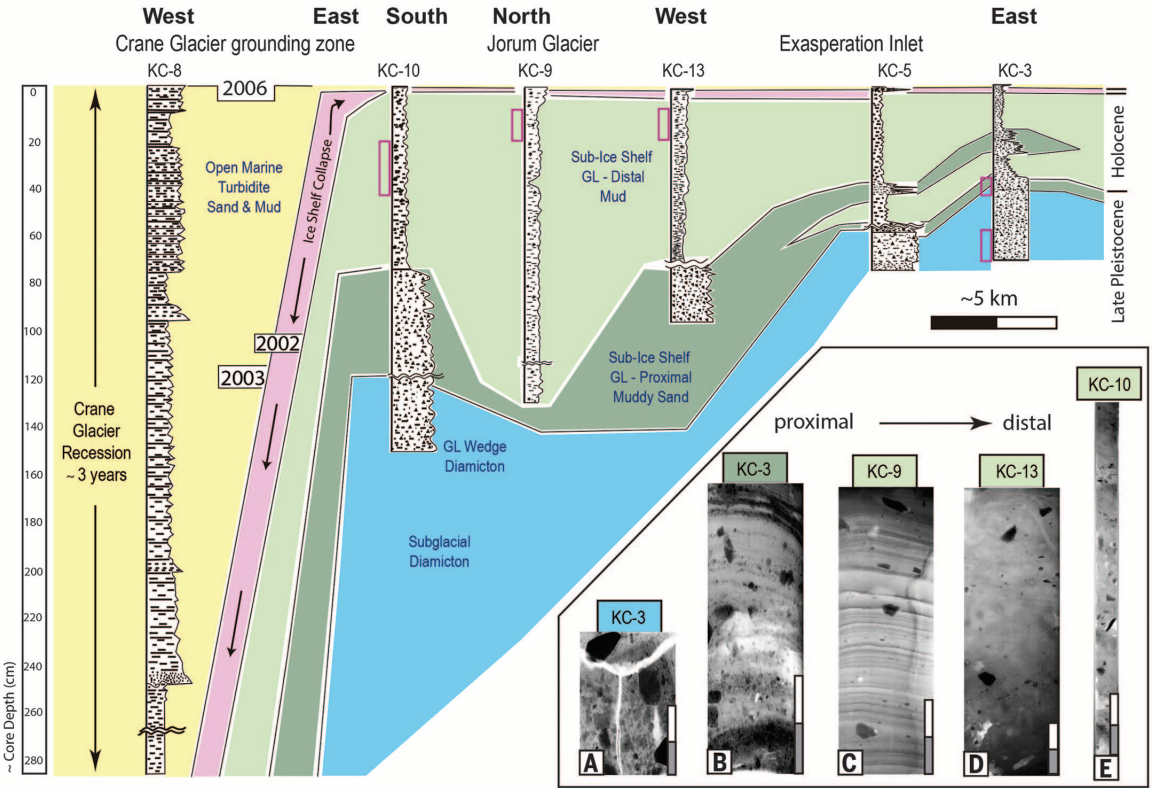

Fig. 3. Fence diagram of core sites and stratigraphic model across the grounding line wedge with sequence of events related to collapse of LIS-B. Facies correlation among cores is shown with color scheme. GL, grounding line. (Inset) X-ray radiograph positives (clasts are opaque) of specific facies intervals in selected cores. Red rectangles next to each core indicate position of each x-ray radiograph. Scale bar, 5 cm. Proximal to distal positions relative to grounded ice are shown for the sequence of x-ray radiographs as left to right, respectively.

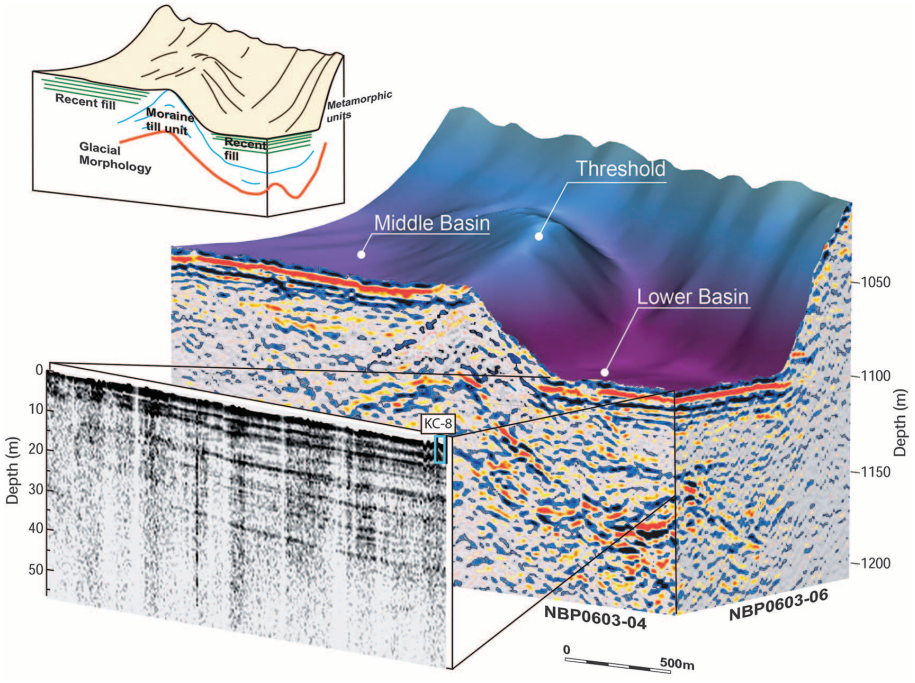

Fig. 4. Three-dimensional view of seismic reflection data and multibeam bathymetry from Crane Fjord. Seismic line locations are shown in Fig. 1, inset. Colored reflectors in block diagram are from Generator Injector Air Gun–seismic reflection, and the grayscale panel is from a 3.5 kHz compressed high-intensity radar pulse subbottom system. (Inset) Line drawing interpretation of layered and chaotic reflectors.

summer 2002–2003 (3 years before core recovery). In general, *Fragilariopsis* comprise >80% of the diatom assemblage, and in half the samples, this genus comprises >90% of the diatom assemblage (tables S2 and S3). Preservation is excellent, with many very lightly silicified specimens occurring in ribbon colonies containing chloroplasts. Although diatoms can be advected underneath ice shelves (*23*), data indicate that advection of diatoms has not been observed beneath the LIS-B (*11*, *24*). Our observations as well suggest the absence of advection of diatoms underneath the LIS-B because these cores also document the opening of the Larsen B embayment, the associated increase in diatom abundance, and the lack of diatoms below the uppermost part of the cores, except in NBP0603 KC-8 (Fig. 2). The pristine condition of the frustules coincides with high water content with generally finer grain size, pointing to the very recent and rapid deposition of the valves at the sea floor and very limited transport. This core is interpreted to represent just over 1 year of deposition (from austral summer 2004–2005 to the end of the austral summer 2005–2006), with an extraordinary sedimentation rate of about 2 m/year (Fig. 3 and fig. S2). The sandy intervals are interpreted as summer turbidites, deposited when open water and surface melt would contribute to slope instabilities along the walls of the fjord and within the glacier terminus system (Figs. 2 and 3 and fig. S2).

Downward extrapolation of the ~2 m/year sedimentation rate estimated from core KC-8 suggests that only the uppermost ~6 m of sediment in the lower basin were deposited after LIS-B breakup, corresponding to the layered reflectors ("recent fill") identified in the seismic reflection data (Figs. 3 and 4). The remainder of the sediments imaged in the lower basin,

~35 m thick, may correspond to a sequence of turbidites, as observed in other grounding zone proximal sites (*25*). The ponded morphology and acoustic stratification of the sediments support this interpretation (Figs. 1 and 4). The middle basin likely contains a sediment sequence similar to that observed in the lower basin. In its position landward of the 2001 grounding zone (Fig. 1), the deep upper basin may have existed as a subglacial lake through the Holocene (*21*).

As estimates for projected sea-level rise over the next century continue to be revised from recent Intergovernmental Panel on Climate Change forecasts, the stability of GZSs need further evaluation. Relict GZSs now observed from several offshore troughs on the Antarctic continental shelf record a time of extreme rates of sea-level change in the Quaternary (*19*, *26*, *27*). Yet, "modern" GZSs found near critical regions are interpreted to have been abandoned within recent decades, which is coincident with feedbacks in ice-shelf basal melting, grounding line recession, and ice-sheet thinning (*28*). The stability of the LIS-B with its GZS through the Holocene and their recent rapid collapse suggests strong sensitivity to surface warming. This adds to the scenario of instability now facing Antarctic glacial masses and must invigorate continued examination of GZS in spite of difficulty in access, logistical risk, and competing resources.

REFERENCES AND NOTES

1. R. B. Alley, P. U. Clark, P. Huybrechts, I. Joughin, *Science* **310**, 456–460 (2005).
2. E. C. King, R. C. A. Hindmarsh, C. R. Stokes, *Nat. Geosci.* **2**, 585–588 (2009).
3. M. Oppenheimer, *Nature* **393**, 325–332 (1998).
4. S. Anandakrishnan, G. A. Catania, R. B. Alley, H. J. Horgan, *Science* **315**, 1835–1838 (2007).
5. E. Rignot *et al*., *Geophys. Res. Lett.* **31**, L18401 (2004).
6. T. A. Scambos, J. A. Bohlander, C. A. Shuman, P. Skvarca, *Geophys. Res. Lett.* **31**, L18402 (2004).
7. P. Skvarca, H. De Angelis, A. F. Zakrajsek, *Ann. Glaciol.* **39**, 557–562 (2005).
8. T. Scambos, C. Hulbe, M. Fahnestock, in *Antarctic Peninsula Climate Variability: Historical and Paleoenvironmental Perspectives*, E. Domack, A. Burnett, A. Leventer, P. Conley, M. Kirby, R. Bindschadler, Eds., *Antarctic Research Series*, **79**, 79–92 (2003).
9. C. L. Hulbe, T. A. Scambos, T. Youngberg, A. K. Lamb, *Global Planet. Change* **63**, 1–8 (2008).
10. E. Rignot, *Philos. Trans. A Math. Phys. Eng. Sci.* **364**, 1637–1655 (2006).
11. E. Domack *et al*., *Nature* **436**, 681–685 (2005); see cover photo of issue.
12. M. Canals, R. Urgeles, A. M. Calafat, *Geology* **28**, 31–34 (2000).
13. A. Camerlenghi *et al*., *Mar. Geophys. Res.* **22**, 417–443 (2001).
14. W. Rack, H. Rott, *Ann. Glaciol.* **39**, 505–510 (2004).
15. J. Evans, C. J. Pudsey, C. O'Cofaigh, P. Morris, E. W. Domack, *Quat. Sci. Rev.* **24**, 741–774 (2005).
16. E. W. Domack, E. A. Jacobson, S. S. Shipp, J. B. Anderson, *Geol. Soc. Am. Bull.* **111**, 1517–1536 (1999).
17. M. Rebesco *et al*., *Mar. Geol.* **279**, 141–147 (2011).
18. D. E. Sugden, B. S. John, *Glaciers and Landscape: A Geomorphologic Approach* (Edward Arnold, London, 1976).
19. E. Domack *et al*., *Geomorphology* **75**, 125–142 (2006).
20. J. B. Anderson, in *The Geology of Antarctica*, R. J. Tingey, Ed. (Clarendon Press, Wotton-under-Edge, 1991), pp. 285–334.
21. T. A. Scambos, E. Berthier, C. A. Shuman, *Ann. Glaciol.* **52**, 74–82 (2011).
22. M. Rebesco, A. Camerlenghi, L. De Santis, E. Domack, M. Kirby, *Mar. Geol.* **151**, 89–110 (1998).
23. A. L. Post, M. A. Hemer, P. E. O'Brien, D. Roberts, M. Craven, *Mar. Ecol. Prog. Ser.* **344**, 29–37 (2007).
24. E. Sañé, E. Isla, M. A. Bárcena, D. J. DeMaster, *PLOS One* **8**, e52632 (2013).
25. E. W. Domack, S. E. Ishman, *Geol. Soc. Am. Bull.* **105**, 1175–1189 (1993).
26. K. McMullen *et al*., *Palaeogeogr. Palaeocl.* **231**, 169–180 (2006).
27. J. B. Anderson, *Science* **315**, 1803–1804 (2007).
28. A. Jenkins *et al*., *Nat. Geosci.* **3**, 468–472 (2010).

ACKNOWLEDGMENTS

We thank the shipboard participants, captain, and crew of cruises NBP0603 and LMG0502 and the staff at the Antarctic Marine Geology Research Facility, Florida State University. This project was supported by grants from the NSF–Office of Polar Programs (0732467 to E.D.; 0732625 to A.L.; 0732605 to S.B.) and from Italian Programma Nazionale di Ricerche in Antartide project ULISSE. The data reported in this paper are tabulated in the supplementary materials. M.R. collected and interpreted seismic reflection data aboard cruise NBP0603 and assisted with writing major portions of the manuscript. E.D. supervised collection of field data and sedimentologic core data for cruises LMG0502 and NBP0603, wrote major portions of the paper, and drafted Figs. 2 and 3. F.Z. collected, processed, and interpreted seismic reflection data aboard cruise NBP0603 and wrote sections of the paper dealing with interpretation of the reflection data. C.L. processed multibeam data, drafted Fig. 1, and wrote sections of the paper dealing with multibeam data. A.L. helped collect data aboard LMG0502 and NBP0603, analyzed diatom abundance data, and wrote sections of the paper dealing with diatom abundance and interpretation. S.B. helped collect data aboard NBP0603, collected and analyzed magnetic susceptibility data, and wrote sections of the paper dealing with physical properties of sediment cores. V.W. assisted in collecting sediment cores during LMG0502, collected color images of sediment cores during this cruise, and helped to draft portions of Fig. 2. G.H. assisted in collecting sediment cores during NBP0603, provided color images of sediment cores collected in this cruise, and helped with editing the manuscript. M.T. imported air geophysical data for interpretation of longitudinal profile of the Crane Glacier and provided editing of the manuscript. T.S. imported remote sensing data and interpretation of grounding line fluctuation before and after ice shelf collapse and assisted in writing and editing the paper. J.S. participated in collecting sediment cores and other data during LMG0502 and assisted in writing and editing the paper. E.P. was instrumental in the extensive discussion related to supplemental material dealing with ice terraces and morainal debris.

SUPPLEMENTARY MATERIALS

www.sciencemag.org/content/345/6202/1354/suppl/DC1
Materials and Methods
Figures S1 and S2
Tables S1, S2 and S3
References (*29*–*31*)

29 May 2014; accepted 1 August 2014
10.1126/science.1256697

FISH PIGMENTATION

Thyroid hormone–dependent adult pigment cell lineage and pattern in zebrafish

Sarah K. McMenamin,[1] Emily J. Bain,[1] Anna E. McCann,[1] Larissa B. Patterson,[1] Dae Seok Eom,[1] Zachary P. Waller,[1] James C. Hamill,[1] Julie A. Kuhlman,[2] Judith S. Eisen,[3] David M. Parichy[1,4]*

Pigment patterns are useful for elucidating fundamental mechanisms of pattern formation and how these mechanisms evolve. In zebrafish, several pigment cell classes interact to generate stripes, yet the developmental requirements and origins of these cells remain poorly understood. Using zebrafish and a related species, we identified roles for thyroid hormone (TH) in pigment cell development and patterning, and in postembryonic development more generally. We show that adult pigment cells arise from distinct lineages having distinct requirements for TH and that differential TH dependence can evolve within lineages. Our findings demonstrate critical functions for TH in determining pigment pattern phenotype and highlight the potential for evolutionary diversification at the intersection of developmental and endocrine mechanisms.

Vertebrates exhibit a stunning variety of pigment patterns, yet the mechanisms underlying pattern development and evolution are only beginning to be discovered. Among the most conspicuous and elaborate patterns are those of teleost fishes, which function in mate choice, shoaling, camouflage, and speciation (*1*–*3*). In the zebrafish *Danio rerio*, the adult pattern comprises dark stripes of black melanophores and a few iridescent iridophores, alternating with light "interstripes" of yellow/orange xanthophores and abundant iridophores, all within the hypodermis, between the epidermis and myotome (*4*) (Fig. 1A). Short-range and

[1]Department of Biology, University of Washington, Seattle, WA 98195, USA. [2]Genetics, Development and Cell Biology, Iowa State University, Ames, IA 50011, USA. [3]Institute of Neuroscience, University of Oregon, Eugene, OR 97403, USA. [4]Institute for Stem Cell and Regenerative Medicine, UW Medicine Research, Seattle, WA 98109, USA.
***Corresponding author. E-mail: dparichy@u.washington.edu**